Cell

A Structural Basis for the Assembly and Functions of a Viral Polymer that Inactivates Multiple Tumor Suppressors

Horng D. Ou,[1] Witek Kwiatkowski,[2] Thomas J. Deerinck,[5] Andrew Noske,[5] Katie Y. Blain,[2] Hannah S. Land,[3] Conrado Soria,[1] Colin J. Powers,[1] Andrew P. May,[10] Xiaokun Shu,[7,8,11] Roger Y. Tsien,[7,8,9] James A.J. Fitzpatrick,[4] Jeff A. Long,[3] Mark H. Ellisman,[5,6] Senyon Choe,[2] and Clodagh C. O'Shea[1,*]
[1]Molecular and Cell Biology Laboratory
[2]Structural Biology Laboratory
[3]Plant Biology Laboratory
[4]Waitt Advanced Biophotonics Center
Salk Institute for Biological Studies, 10010 North Torrey Pines Road, La Jolla, CA 92037, USA
[5]National Center for Microscopy and Imaging Research, Center for Research in Biological Systems
[6]Department of Neurosciences
[7]Howard Hughes Medical Institute
[8]Department of Pharmacology
[9]Departments of Chemistry and Biochemistry
University of California, San Diego, 9500 Gilman Drive, La Jolla, CA 92093, USA
[10]Fluidigm Corporation, 7000 Shoreline Court, Suite 100, South San Francisco, CA 94080, USA
[11]Department of Pharmaceutical Chemistry and Cardiovascular Research Institute, University of California, San Francisco, 555 Mission Bay Boulevard South, San Francisco, CA 94158, USA
*Correspondence: oshea@salk.edu
http://dx.doi.org/10.1016/j.cell.2012.08.035

SUMMARY

Evolution of minimal DNA tumor virus' genomes has selected for small viral oncoproteins that hijack critical cellular protein interaction networks. The structural basis for the multiple and dominant functions of adenovirus oncoproteins has remained elusive. E4-ORF3 forms a nuclear polymer and simultaneously inactivates p53, PML, TRIM24, and MRE11/RAD50/NBS1 (MRN) tumor suppressors. We identify oligomerization mutants and solve the crystal structure of E4-ORF3. E4-ORF3 forms a dimer with a central β core, and its structure is unrelated to known polymers or oncogenes. E4-ORF3 dimer units coassemble through reciprocal and nonreciprocal exchanges of their C-terminal tails. This results in linear and branched oligomer chains that further assemble in variable arrangements to form a polymer network that partitions the nuclear volume. E4-ORF3 assembly creates avidity-driven interactions with PML and an emergent MRN binding interface. This reveals an elegant structural solution whereby a small protein forms a multivalent matrix that traps disparate tumor suppressors.

INTRODUCTION

Viral proteins offer a rich underexplored structural landscape in which to discover optimized designs that target critical cellular pathways. The higher replication and mutation rate of viruses enables rapid protein evolution and exhaustive optimization. Viral proteins can also explore physical forms forbidden to cellular proteins because they do not have to be compatible with the continued existence of the host; they just have to win. Adenovirus is a small DNA tumor virus (<40 kb) that expresses 11 "early" E1 and E4 proteins that take over human cells, forcing cells to propagate the viral genome and proteins (Berk, 2007). Adenoviral early proteins achieve this by usurping the interactions of multiple cellular targets that regulate growth and survival (Weitzman and Ornelles, 2005). Elucidating the interactions of adenoviral early proteins has been a powerful biochemical strategy with which to discover key cellular targets and mechanisms that are also deregulated in cancer, such as the RB/p107/p130 family of tumor suppressors, E2F and p300 (O'Shea, 2005). Adenoviral oncoproteins' functions are all the more impressive when realizing that the majority of them are less than 20 kDa (the average human protein size is 53 kDa) and have little detectable sequence similarity to human proteins. This suggests that they have found novel or optimized solutions to interact with many different cellular protein hubs. However, no full-length adenoviral oncoprotein structures have been solved (Ou et al., 2011). Thus, the structural basis for their functions remains unknown. This represents a fundamental gap in our understanding of adenovirus, a global human pathogen and one of the predominant viral vectors used in both basic research and gene therapy.

Elucidating the structure of adenoviral early proteins also has a much broader impact. The rational design of small molecules and proteins that disrupt the interactions of large cellular protein-protein interaction complexes is a major challenge (Wells

and McClendon, 2007). Cellular multifunctional protein interaction hubs (Vidal et al., 2011) generally have large molecular weights (>70 kDa) (Patil et al., 2010) that accommodate multiple modular domains (Scott and Pawson, 2009) and/or local intrinsic disordered regions to interact with many different binding partners (Haynes et al., 2006). Based on this, it would be easy to conclude that it is neither conceptually nor practically possible to design small proteins that disrupt multiple large protein complexes. The structures and functions of adenoviral oncoproteins could reveal new strategies for designing small proteins that disrupt multiple large protein complexes.

Adenovirus E4-ORF3 is a small 116 residue (13 kDa) protein that challenges our current understanding of the requisite properties of polymers and multifunctional protein-protein interaction hubs. E4-ORF3 binds and inactivates multiple disparate tumor suppressors and forms a remarkable network of cables that weaves through the nucleus (Carvalho et al., 1995; Doucas et al., 1996; Soria et al., 2010; Yondola and Hearing, 2007). In contrast to actin and microtubules, which form uniform linear filaments (Chhabra and Higgs, 2007; Howard and Hyman, 2003), E4-ORF3 forms highly irregular cable-like assemblies (Carvalho et al., 1995; Doucas et al., 1996; Soria et al., 2010). This suggests that E4-ORF3 is structurally distinct from cellular polymers. However, the ultrastructure of E4-ORF3 assemblies remains unknown.

The pleiotropic biological functions of E4-ORF3 include suppression of the interferon response (Ullman et al., 2007), stimulation of viral RNA splicing (Nordqvist et al., 1994), and prevention of viral genome concatenation (Stracker et al., 2005). E4-ORF3 binds and disrupts large cellular protein complexes, including PML bodies (Doucas et al., 1996), the MRE11/RAD50/NBS1 (MRN) DNA repair complex (Stracker et al., 2002), and TRIM24 (Yondola and Hearing, 2007). PML, MRN complex components, and TRIM24 are important tumor suppressors that are inactivated by mutations in several different cancers (Bernardi and Pandolfi, 2007; D'Amours and Jackson, 2002; Khetchoumian et al., 2007). Recently, E4-ORF3 was discovered to inactivate p53 tumor suppressor functions by specifying repressive heterochromatin assembly at p53 target promoters, thereby preventing p53-DNA binding (Soria et al., 2010). The structural basis for E4-ORF3's multiple functions and inactivation of disparate tumor suppressors is not understood.

Here, we show that E4-ORF3 self-assembles to form a polymer network in both plants and human cells. We identify dominant-negative oligomerization mutants to solve the structure of an E4-ORF3 dimer at 2.1 Å resolution. E4-ORF3 structure is not related to that of known cellular oncogenes or polymer-forming proteins but has a similar β core dimeric motif to that of the DNA binding domain (DBD) of human papillomavirus 16 (HPV16) E2. Based on structural, mutagenesis, and functional analyses, we provide a model for E4-ORF3 assembly, namely that E4-ORF3 dimer units can coassemble through reciprocal and nonreciprocal exchanges of their C-terminal tails. Using a genetically encoded tag for electron microscopy (EM), we show that E4-ORF3 polymers are disordered weaves of linear and branched oligomer threads that form a 3D network that partitions the nucleus around viral replication domains. E4-ORF3 assembly is a unifying mechanism required for inactivating PML, MRN, and p53 to facilitate viral replication. We demonstrate that E4-ORF3 higher-order assembly creates avidity-driven interactions with PML and an emergent MRN binding interface at residues V^{101}–D^{105} in the C-terminal tail. Together, our studies reveal a small-ordered protein structure and assembly mechanism that binds and disrupts multiple large tumor suppressor complexes.

RESULTS

E4-ORF3 Self-Assembles to Form an Irregular Polymer Network in Both Human and Plant Cells

E4-ORF3 forms unusual "track"-like superstructures in the nucleus (Carvalho et al., 1995; Doucas et al., 1996; Soria et al., 2010). Due to the limited resolution of light microscopy, it is unclear if E4-ORF3 tracks are assemblies of multiple individual fibers or a continuous polymer network. To investigate this further, we applied super-resolution-structured illumination microscopy (SR-SIM) (Gustafsson, 2000). E4-ORF3 forms highly irregular looping cable-like assemblies adjacent to dense cellular DNA superstructures that appear to be a single continuous polymer structure at resolutions of approximately 100 nm (Figure 1A).

An important question is if E4-ORF3 requires accessory human factors, such as an underlying nuclear architecture, cellular interacting proteins, or DNA to assemble. There are no plant homologs of the known E4-ORF3-interacting proteins. Therefore, we expressed E4-ORF3 as a GFP fusion protein in *Nicotiana benthamiana* (tobacco). E4-ORF3-GFP is of a sufficiently large size to be excluded from the nucleus but assembles into a network of cables in the cytoplasm of *Nicotiana* cells that is macroscopically similar to the structure it forms in the nucleus of human cells (Figure 1B). We conclude that E4-ORF3 requires neither nuclear localization nor accessory human factors to self-assemble. Furthermore, these data demonstrate that E4-ORF3 is able to assemble even when it is fused to a protein that is three times its size.

A Dominant-Negative Oligomerization Mutant that Prevents E4-ORF3 Higher-Order Assembly and Is Amenable to Structural Determination

The ability of E4-ORF3 to assemble in plants indicates that all the necessary instructions for forming higher-order superstructures are encoded within individual E4-ORF3 molecules. Therefore, the atomic structure of E4-ORF3 is key to understanding both its assembly and functions. Self-assembling polymeric proteins present a notorious obstacle for structural analyses. E4-ORF3 is not an exception, and the wild-type (WT) protein forms insoluble aggregates when expressed in *E. coli* (data not shown). Therefore, to solve the structure of E4-ORF3, we had to first find a mechanism to isolate soluble oligomeric units and prevent their polymerization.

As an initial step, we established an immunofluorescence assay in human cells to monitor the coassembly of WT E4-ORF3. When coexpressed together in U2OS cells, myc and flag epitope-tagged E4-ORF3 proteins coassemble into a supramolecular scaffold (Figure 1C). This provided a cell-based assay to identify mutations that prevent E4-ORF3 assembly. Previous alanine-scanning mutagenesis of E4-ORF3 showed that substitution of the conserved N^{82} residue (Figure 1D) resulted in diffuse

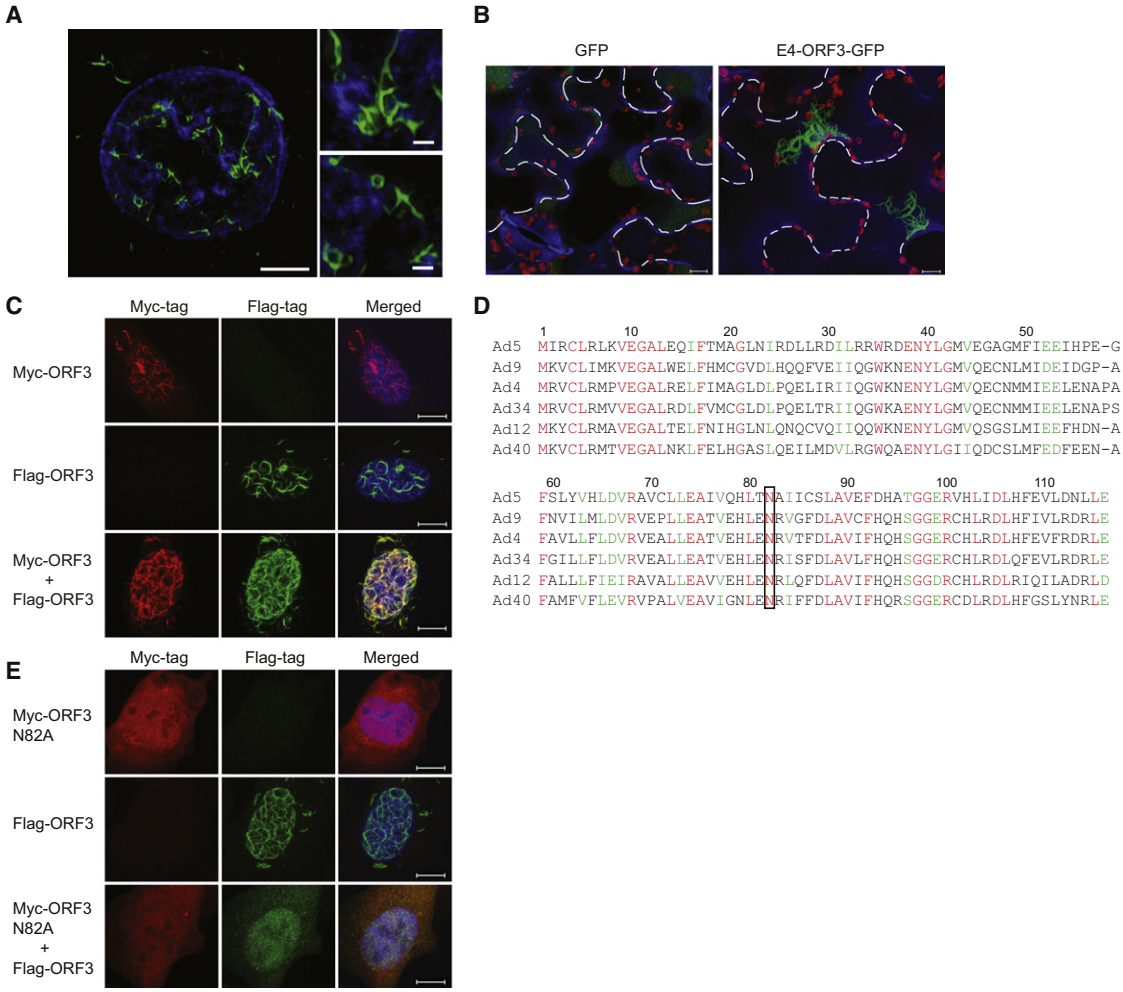

Figure 1. E4-ORF3 Self-Assembly Is Prevented by N^{82} Dominant-Negative Oligomerization Mutations

(A) SR-SIM image of Ad5-infected primary SAECs at 36 hr postinfection (hpi). E4-ORF3 is in green, DNA in blue.

(B) GFP (left) and E4-ORF3-GFP (right) in *Nicotiana benthamiana* leaf epidermal cells. The cell wall (outlined with a dashed white line) is stained in blue, and plastid autofluorescence is red.

(C) U2OS cells transfected with either myc-tagged E4-ORF3 (red), flag-tagged E4-ORF3 (green) or both together. DNA is counterstained with Hoechst (blue).

(D) Sequence alignment of E4-ORF3 from distal human adenoviral serotypes. The black box marks the conserved N^{82} residue.

(E) U2OS cells transfected with either myc-tagged E4-ORF3 N82A (red), flag-tagged E4-ORF3 (green) or an equal amount of both.

Scale bars, 5 and 1 μm (A) and 10 μm (B, C, and E). See also Figure S1.

nuclear and cytoplasmic staining (Evans and Hearing, 2003; Hoppe et al., 2006; Stracker et al., 2002). A trivial explanation for this phenotype is that N82A mutations result in protein misfolding. However, an alternative explanation is that N82A mutations disrupt oligomeric interactions necessary for E4-ORF3 assembly. We reasoned that if E4-ORF3 N82A is folded it might act as a dominant-negative oligomerization mutant and disrupt the assembly of WT E4-ORF3. Consistent with this, when coexpressed together, myc-tagged E4-ORF3 N82A is dominant and prevents the assembly of flag-tagged WT E4-ORF3 (Figure 1E).

The identification of the dominant-negative oligomerization properties of N82A mutants provided a mechanism for isolating E4-ORF3 oligomeric units for structure determination. Unlike WT E4-ORF3, the expression of E4-ORF3 N82A in *E-coli* yields soluble protein that has a molecular weight consistent with a dimer (see Figure S1A available online). Further protein engineering was required to produce crystals that yielded high-resolution diffraction data: C^{71} and C^{86} were each changed to serine to prevent nonspecific disulfide crosslinking, and N^{82} was substituted with glutamic acid to enhance protein solubility. The E4-ORF3 N82E/C71S/C86S triple mutant (abbreviated as E4-ORF3 N82*) eluted as a homogeneous protein dimer (Figure S1B) and had the same dominant-negative properties as an N82A single mutant when coexpressed with WT E4-ORF3 (Figure S1C). In contrast, C71S/C86S double mutant does not prevent E4-ORF3 assembly (Figure S1D). We obtained high-quality crystals of seleno-methionine-labeled E4-ORF3 N82* and determined the structure at 2.1 Å resolution using single-wavelength anomalous dispersion phasing (Table S1).

Crystal Structure of an E4-ORF3 Dimer

E4-ORF3 forms a dimer comprising three helices (α1, α2, and α3) that pack against three antiparallel β strands (β1, β2, and β3) followed by a "C-terminal tail" (amino acid residues 99–116) containing a short β4 strand (Figures 2A and 2B). The β1–β3 strands form the dimer interface, centered around a cluster of hydrophobic residues I^2, C^4, F^{50}, Y^{62}, and H^{64}, with polar residues R^6, E^{52}, and S^{60} at the bottom (Figure 2C). The dimeric β core is sealed at the front and back via L^{111} in the β4 strand (Figures 2A and 2B). This is achieved by the bending back of the C-terminal tail at a hinge region that comprises the highly conserved ^{96}TGGER^{100} residues (Figures 2A and 2B). The surface area of the β core dimerization interface (~1,504 Å^2) is close to that observed in obligate dimers (~1,712 Å^2) (Ponstingl et al., 2000) and comprises 25% of the total surface area of each E4-ORF3 dimer subunit. This suggests that E4-ORF3 is an obligate dimer and that dimerization is the first-order event for higher-order assembly.

E4-ORF3 specifies repressive heterochromatin assembly at p53 target genes (Soria et al., 2010), suggesting that it may be a direct DNA binding protein. However, DNA binding proteins generally have a neutral or basic pI and electropositive clusters on their surface (Brendel and Karlin, 1989). In contrast, E4-ORF3 has an acidic pI (5.1), and the dimer has an electronegative surface potential (Figure 2D). This suggests that E4-ORF3 acts through intermediaries to silence p53 target genes or that the assembly of E4-ORF3 dimer units creates an emergent DNA binding surface.

E4-ORF3 Structural Homologs

Structural comparisons using Dali (Holm and Rosenström, 2010) and PDBeFOLD (Krissinel and Henrick, 2004) servers show that the structure of E4-ORF3 is distinct from that of known cellular polymers or proteins that function in the p53, PML, DNA damage, and TRIM24 tumor suppressor pathways. E4-ORF3 resembles proteins that have a ferredoxin-like fold. The top hit in the Dali search was the *Helicobacter pylori* IS*Hp608* TnpA DNA transposase (Ronning et al., 2005). However, TnpA and E4-ORF3 have very different dimerization mechanisms, sequences, surface charges, and functions (Figures S2A–S2C). TnpA has been suggested to have a similar topology to the RNA recognition motif (RRM) (Ronning et al., 2005). E4-ORF3 also resembles the RRM topology (β1α1β2β3α2β4) but has an additional α2 helix (Figure S2D). Furthermore, in E4-ORF3 the β sheet is used for dimerization as opposed to nucleic acid binding.

Strikingly, PDBeFOLD searches revealed that the DBD of the HPV16 E2 protein (Hegde and Androphy, 1998) is a structural homolog of E4-ORF3. E2 is a master viral transcription factor that has a modular structure, comprising an N-terminal transactivation domain linked to the C-terminal DBD (Giri and Yaniv, 1988). The superimposed structures of E4-ORF3 and E2 DBD have a root-mean-square deviation (rmsd) of 2.9 Å with 72 structurally equivalent residue pairs (Figure 2E). However, only 9% of their amino acids are identical (Figure 2F). The E2 DBD dimer has an electropositive surface (Figure 2G) and binds to DNA via residues in the two α1 helices and the loop between β2 and β3 (Hegde and Androphy, 1998; Kim et al., 2000). The DNA binding residues and α1 helices are located on the same face of the dimer to bind palindromic sequences in the HPV genome (Figure 2G). Only three out of the eight E2 DBD α1 DNA binding residues are conserved in the corresponding α2 helix of E4-ORF3 (Figure 2F). Furthermore, the α2 helices are on opposite faces of the E4-ORF3 dimer (Figure 2A).

Although their functions with respect to DNA binding may differ, it is conspicuous that both E4-ORF3 and HPV16 E2 DBD dimerize through a central β core (Figures 2A and 2G). Furthermore, the β core dimeric motif is also common to another DNA tumor virus protein, the Epstein-Barr virus EBNA1 DBD (Figure 2G) (Bochkarev et al., 1995). However, neither E2 DBD nor EBNA1 DBD dimers assemble to form a supramolecular structure similar to E4-ORF3.

E4-ORF3 Dimer Units Assemble through Intermolecular Exchange of Their C-Terminal Tails

The dominant-negative oligomerization properties of E4-ORF3 N82* provide a functional assay to determine the structural basis of WT E4-ORF3 assembly. N^{82} is in the middle of α3 and solvent exposed (Figure 2A), suggesting that it is at a critical α3 interface that is required for the assembly and stacking of E4-ORF3 polymers. To test this, we mutated α3 residues that are on the same helical "face" as N^{82} or similarly conserved (Figures 3A and S3A). In contrast to N82A (Figure 1E), alanine substitutions of adjacent and conserved residues in α3 do not prevent E4-ORF3 higher-order assembly (Figures S3B and S3C). However, C86A mutants exhibit some diffuse background staining compared to WT E4-ORF3, suggesting that C^{86} may have a secondary role in stabilizing E4-ORF3 assemblies (Figure S3B). These data do not provide evidence for an extended α3 oligomeric interface having a direct or critical role in E4-ORF3 assembly. This led us to determine if N^{82} mutations indirectly perturb distal oligomeric interactions that are necessary for higher-order assembly.

Structural studies of oligomeric proteins have revealed three mechanisms underlying the specific self-association of proteins to form filaments, fibrils, or aggregates: end-to-end stacking (actin and tubulin) (Chhabra and Higgs, 2007; Howard and Hyman, 2003); cross β-spine (amyloid and amyloid-like proteins) (Sipe and Cohen, 2000); and 3D domain swapping (for example, RNase A) (Bennett et al., 2006). End-to-end stacking and cross-β-spine assembly mechanisms result in linear fibrils and aggregates, respectively. However, E4-ORF3 assemblies are irregular with variable curvatures and loops (Figure 1A). Furthermore, the ability of E4-ORF3 to assemble when it is fused to GFP is not consistent with end-to-end stacking and indicative of a flexible assembly with relaxed packing constraints (Figure 1B).

In 3D domain swapping, the intermolecular exchange of protein domains between oligomeric units can result in branched irregular aggregates (Bennett et al., 2006). We hypothesized that WT E4-ORF3 dimers coassemble through intermolecular swapping of their C-terminal tails (Figure 3B). Our model suggested that the N^{82} mutation causes a tertiary conformational change that locks the C-terminal tail into a "closed" interaction with the β core that prevents intermolecular exchanges (Figure 3B). An E4-ORF3 N82*-WT heterodimer would have a closed dominant-negative configuration (Figure 3C) in which L^{111} seals the β core at one side, thereby "capping" further assembly.

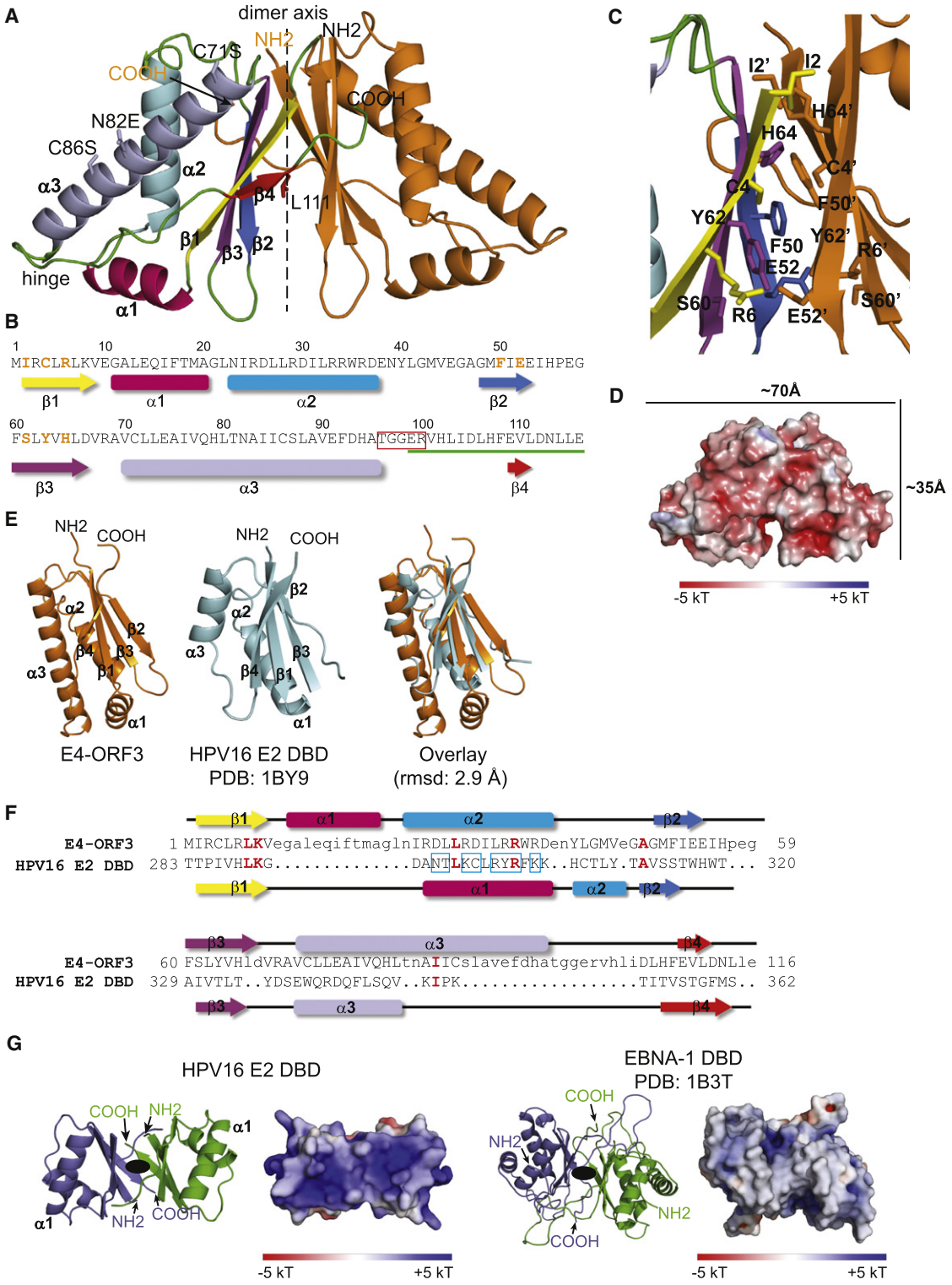

Figure 2. The Crystal Structure of an E4-ORF3 Dimer and Structural Homology to HPV16 E2 DBD

(A) The crystal structure of an E4-ORF3 N82E/C71S/C86S dimer at 2.1 Å resolution.

(B) E4-ORF3 secondary structure elements with corresponding amino acid sequences: β strands are indicated by arrows, α helices by cylinders, β core residues are in orange, C-terminal tail residues are underlined, and hinge residues are indicated by a rectangle.

(C) β Core dimer interface.

(D) Surface electrostatic potential of E4-ORF3 dimer. Red represents a negative charge and blue a positive charge.

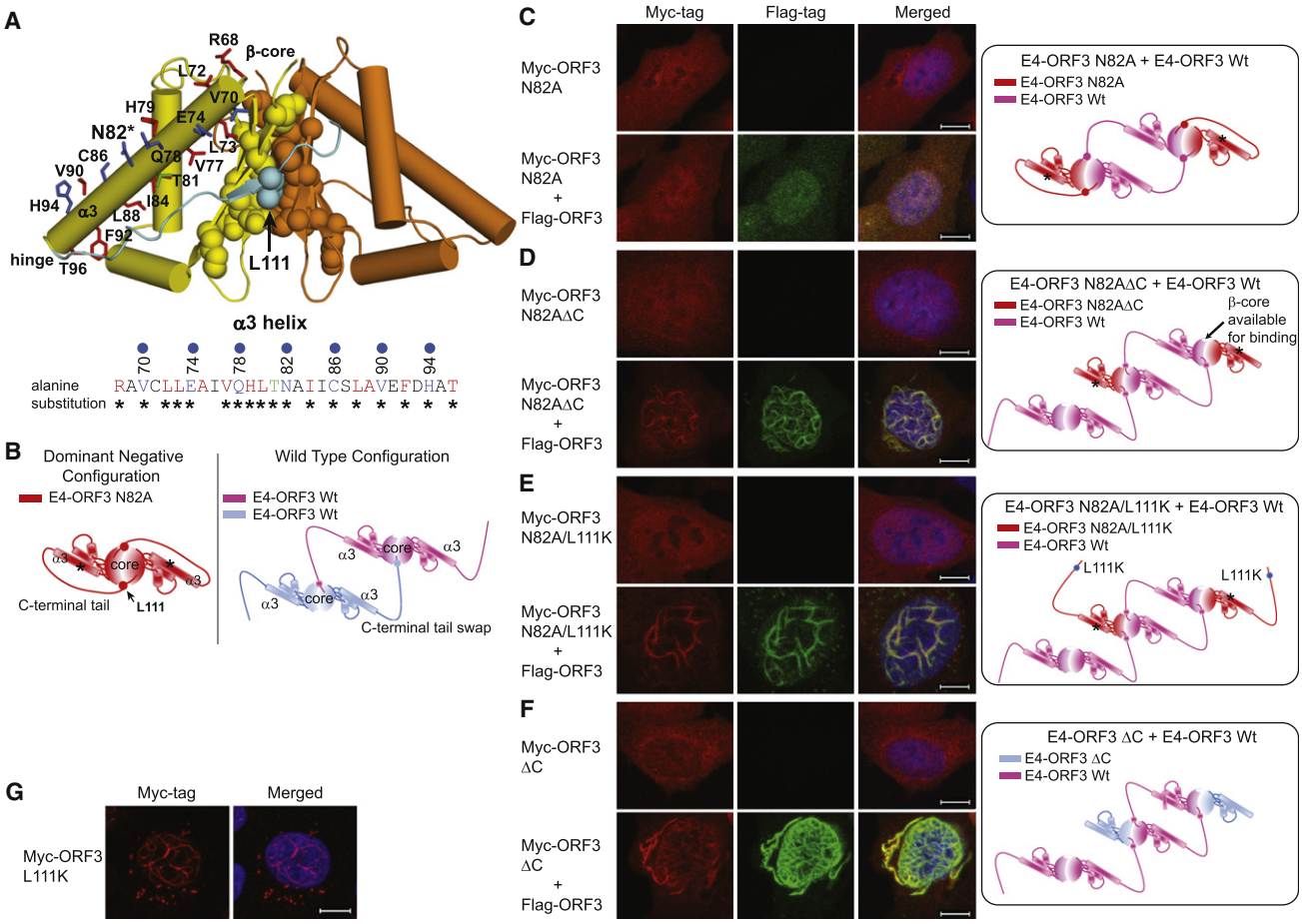

Figure 3. E4-ORF3 Dimers Assemble into a Higher-Order Polymer by Exchanging Their C-Terminal Tails

(A) Space-filling representation of E4-ORF3 N82* dimer structure in which L^{111} (cyan) seals the β core. α3 residues that were mutated to alanine are shown in the model and indicated by an asterisk in the sequence below. Blue dots indicate residues on the same helical face as N^{82}. Conserved residues are labeled red.

(B) Left panel is a top-down representation of the E4-ORF3 N82* dimer structure shown in (A), in which the C-terminal tail is locked into a closed configuration with the β core. The β core is represented by a sphere with a stripe at the dimer interface, the mutated N82 residue is indicated by an asterisk (*), and L111 is depicted as a circle. The right panel is a model for how wild-type E4-ORF3 dimers could further assemble through intermolecular exchanges of their C-terminal tails.

(C–G) U2OS cells transfected with either myc-tagged E4-ORF3 mutants (red), flag-tagged E4-ORF3 (green) or equal amounts of both. Models of mutant and WT E4-ORF3 interactions are shown.

Scale bars, 10 μm. See also Figure S3.

To test our hypothesis and open the β core for intermolecular interactions, we deleted the C-terminal tail (residues 99–116, ΔC) in E4-ORF3 N82A. E4-ORF3 N82AΔC is diffuse; analogous to N82A alone (Figures 3C and 3D). However, in contrast to N82A single mutation, E4-ORF3 N82AΔC is no longer a dominant-negative oligomerization mutant that prevents the assembly of WT E4-ORF3. Instead, E4-ORF3 N82AΔC coassembles with WT E4-ORF3 (Figure 3D). In the crystal structure of E4-ORF3 N82*, L^{111} in the C-terminal tail seals the β core (Figure 3A). Similar to N82AΔC, E4-ORF3 N82A/L111K is not a dominant negative, and its assembly is rescued in *trans* by the coexpression of WT E4-ORF3 (Figure 3E). These data are consistent with our model and demonstrate that N82A mutants are able to coassemble with WT E4-ORF3 when the β core is made available for intermolecular interactions by additional mutations (Figures 3D and 3E).

We next determined if the C-terminal tail is required for WT E4-ORF3 assembly. E4-ORF3 ΔC is diffuse, demonstrating that the

(E) HPV16 E2 DBD is a structural homolog of E4-ORF3 with an rmsd of 2.9 Å.

(F) Alignment of HPV16 E2 DBD and E4-ORF3 sequences based on their structural overlap; identical residues are colored red. Residues that contact DNA in the HPV18 E2 DBD α1 helix are highlighted with a cyan box.

(G) Both HPV16 E2 DBD and EBNA-1 DBD form dimers with a central β barrel and have electropositive surfaces. Dimer axes are perpendicular to the plane of paper (oval).

See also Figure S2 and Table S1.

C-terminal tail is required for E4-ORF3 assembly (Figure 3F). One explanation for this phenotype is that the deletion of the C-terminal tail results in a destabilized E4-ORF3 dimer or protomer. However, E4-ORF3 ΔC assembly is rescued by the coexpression of full-length E4-ORF3 (Figure 3F). These data argue that E4-ORF3 ΔC at least forms heterodimers with the WT protein. Furthermore, these data indicate that E4-ORF3 dimers can coassemble through nonreciprocal C-terminal tail exchanges.

In contrast to the deletion of the C-terminal tail, an L111K mutation does not prevent E4-ORF3 assembly (Figure 3G). Thus, L111K mutations selectively disrupt the interactions of the C-terminal tail with the β core in E4-ORF3 N82* mutants, but not WT E4-ORF3 (Figures 3E and 3G). We conclude that the C-terminal tail is critical for E4-ORF3 higher-order assembly and that N^{82} mutations alter L^{111} interactions with the β core.

WT E4-ORF3 Dimers Have an Extended β4 Strand that Completes the β Barrel to Drive Higher-Order Oligomerization

This failure of L111K to prevent E4-ORF3 assembly is surprising and leads to a major question: What are the molecular interactions between the C-terminal tail and the β core in WT E4-ORF3 that are critical for higher-order assembly? The similar dimerization modes of E4-ORF3 and E2 DBD provided a vital clue. In the E2 DBD dimer, the β4 strand interacts with both β1 and β4′ (Figure 4A), forming a β barrel. In the E4-ORF3 N82* dimer, the β4 strand is short (three residues) and interacts with β1, but not β2′. Based on the E2 DBD dimer structure, we hypothesized that in WT E4-ORF3 the β4 strand is extended, completing the β barrel (Figure 4A). To test this, we made lysine substitutions at individual residues from D^{112} to E^{116} to abolish potential interactions with the hydrophobic β core. D112K, L114K, and E116K mutations do not prevent E4-ORF3 assembly (Figure 4B). In contrast, L115K and N113K prevent E4-ORF3 assembly of a nuclear polymer network and result in diffuse staining or a mixture of diffuse staining with cytoplasmic aggregates, respectively. These results are consistent with residues 109–116 forming an extended β4 strand in WT E4-ORF3, in which every other residue from L^{111} faces the hydrophobic core (Figure 4C). This would change the position of L^{111} and place it more near the base of the β core, which is polar (Figure 4C). This would potentially explain why a L111K mutation does not prevent WT E4-ORF3 higher-order assembly (Figure 3G). Together, these data demonstrate that N^{82} mutations alter the interactions of the C-terminal tail with the β core, thereby preventing higher-order oligomerization.

In 3D domain swapping the exchanged domain is generally at the N or C terminus and linked to the protein core by a flexible "hinge-loop" (Bennett et al., 2006). Therefore, we determined if the glycine residues in the hinge region between α3 and the C-terminal tail facilitate E4-ORF3 higher-order assembly (Figures 2A and 2B). E4-ORF3 $\Delta G^{97}/\Delta G^{98}$ is diffuse but rescued in *trans* by WT E4-ORF3 (Figure 4D). Thus, the hinge residues $G^{97}G^{98}$ are also required for E4-ORF3 assembly.

Model of E4-ORF3 Polymerization

Taken together, we propose the following model: the first-order step in E4-ORF3 assembly is dimerization via β sheet interactions. Dimerization creates new interfaces for higher-order assembly: the front and backside of the dimeric β core. The two β4 strands in each E4-ORF3 dimer can interact with the β cores of adjacent dimers, driving higher-order assembly (Figure 4E). Reciprocal exchanges of the C-terminal tails between dimer units would result in more linear assemblies, whereas nonreciprocal swapping would enable branching. The glycine residues in the hinge of the C-terminal tail could also adopt various backbone dihedral angles, enabling E4-ORF3 domain-swapped dimers to have diverse and flexible orientations. This would result in many different oligomer configurations that could further assemble with each other through avidity-driven interactions (Figure 4E). Our model predicts that E4-ORF3 polymerizes in multiple ways to form a disordered protein superstructure that has multivalent binding sites to interact with many different cellular complexes.

EM Ultrastructure of E4-ORF3 Polymer Assemblies

E4-ORF3 assemblies are refractory to visualization using conventional EM preparations (Carvalho et al., 1995; Morgan et al., 1960; Puvion-Dutilleul et al., 1995), and immunogold labeling is of limited value in elucidating the ultrastructure of polymers. MiniSOG (singlet oxygen generator) is a fluorescent 106-residue protein tag with which to visualize proteins by correlated light and EM (Shu et al., 2011). Fluorescence photo-oxidation of miniSOG catalyzes the local formation of an electron-dense polymer on the surface of the fusion protein that can be detected by EM. Therefore, to visualize E4-ORF3 by EM, we created miniSOG-E4-ORF3 fusion constructs. Our first attempts with N- and C-terminal miniSOG fusions resulted in cytoplasmic aggregates (Figure S4A). Based on the crystal structure of E4-ORF3, we inserted miniSOG in the flexible loop region between α2 and β2 at residue G^{46} (Figure 2B). E4-ORF3 constructs with an internal miniSOG fusion assemble a functional nuclear scaffold that mislocalizes PML, analogous to untagged E4-ORF3 in transfected U2OS cells (Figure S4A). To reveal the ultrastructure of E4-ORF3 in the biologically relevant context of viral infection, we engineered Ad5 viruses that express miniSOG-E4-ORF3 in place of endogenous E4-ORF3 (Figure 5A). The miniSOG-E4-ORF3 nuclear assemblies were photo-oxidized and visualized by correlated light and EM (Figure 5B).

Transmission EM (TEM) images show that E4-ORF3 nuclear assemblies are distinct from cellular polymers, cytoskeletal structures (Aebi et al., 1986), and amyloid-like aggregates (Sipe and Cohen, 2000). E4-ORF3 assemblies are irregular, make U-turns at the nuclear membrane, and form loosely to densely packed bundles (Figures 5C and 5D). A high-resolution tomogram shows that E4-ORF3 polymer assemblies are a weave of what appear to be thin oligomer threads that assemble with one another in no consistent order (Figure 5E; Movie S1). Each slice of the E4-ORF3 tomogram has a distinct pattern. Consistent with our model (Figure 4E), both linear and branched chain configurations are observed, although the former are predominant. Furthermore, individual oligomer threads are not stacked with one another throughout their lengths but appear to associate at multiple points in no fixed geometric arrangement.

E4-ORF3 polymer assemblies do not project in a single plane. Therefore, to reveal the 3D structure and arrangement of

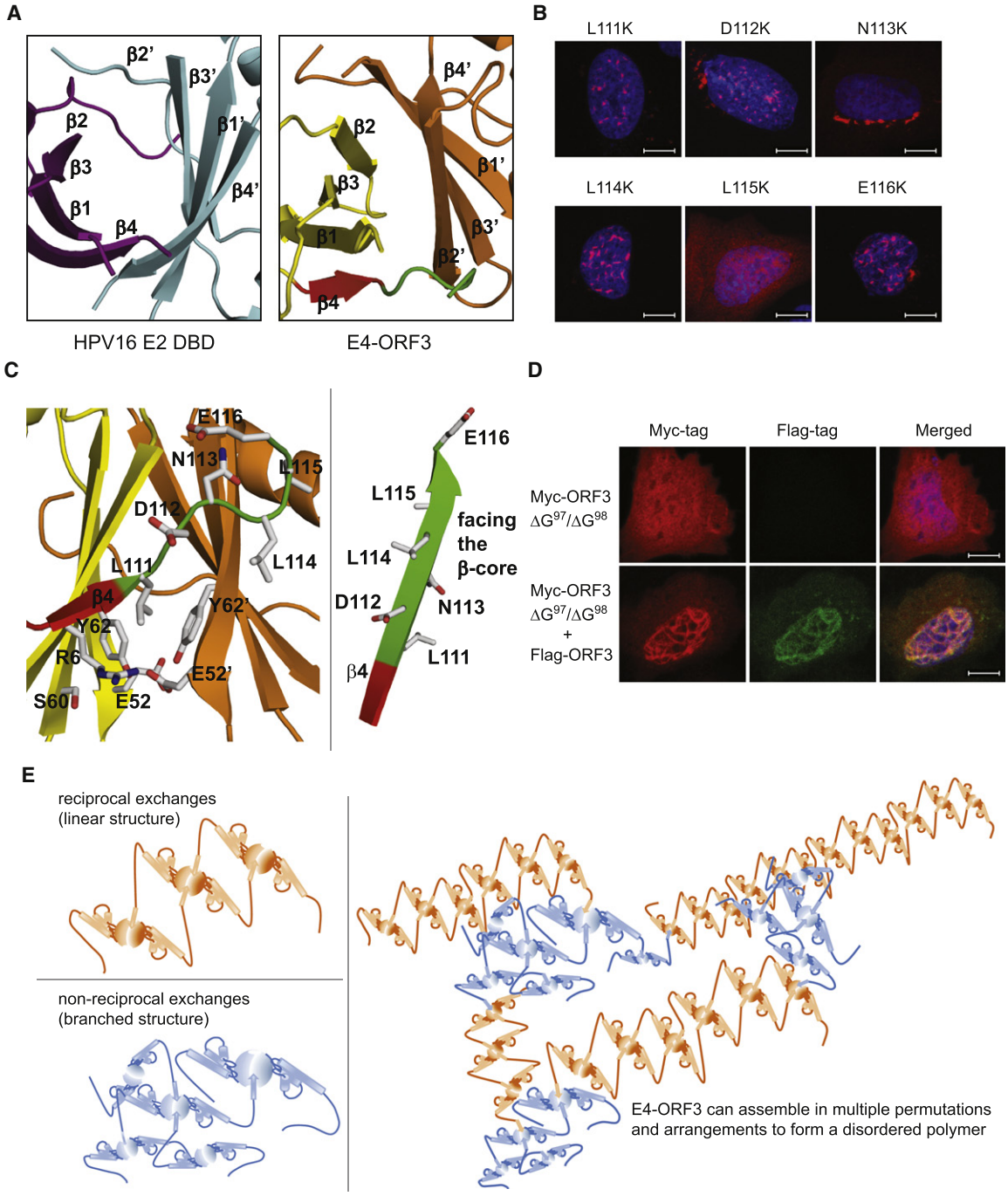

Figure 4. Intermolecular Swapping of an Extended β4 Strand Completes the β Barrel in WT E4-ORF3 Dimers to Drive Higher-Order Oligomerization

(A) In the HPV16 E2 DBD dimer, β4 interacts with both β1 and β4′ to form a β barrel. In the E4-ORF3 N82* dimer, the short β4 strand does not complete the β barrel.

(B) U2OS cells transfected with E4-ORF3 β4 point mutants (red).

(C) In E4-ORF3 N82* a short β4 strand seals the β core through L^{111} interactions (left panel). A model showing that WT E4-ORF3 has an extended β4 strand in which alternating residues face the β core (right panel).

(D) U2OS cells transfected with myc-tagged E4-ORF3 $\Delta G^{97}/\Delta G^{98}$ (red), flag-tagged E4-ORF3 (green), or both.

(E) Model showing E4-ORF3 polymer assembly through a combination of both reciprocal and nonreciprocal C-terminal tail exchanges between dimer units, resulting in linear and branched oligomer chains.

Scale bars, 10 μm.

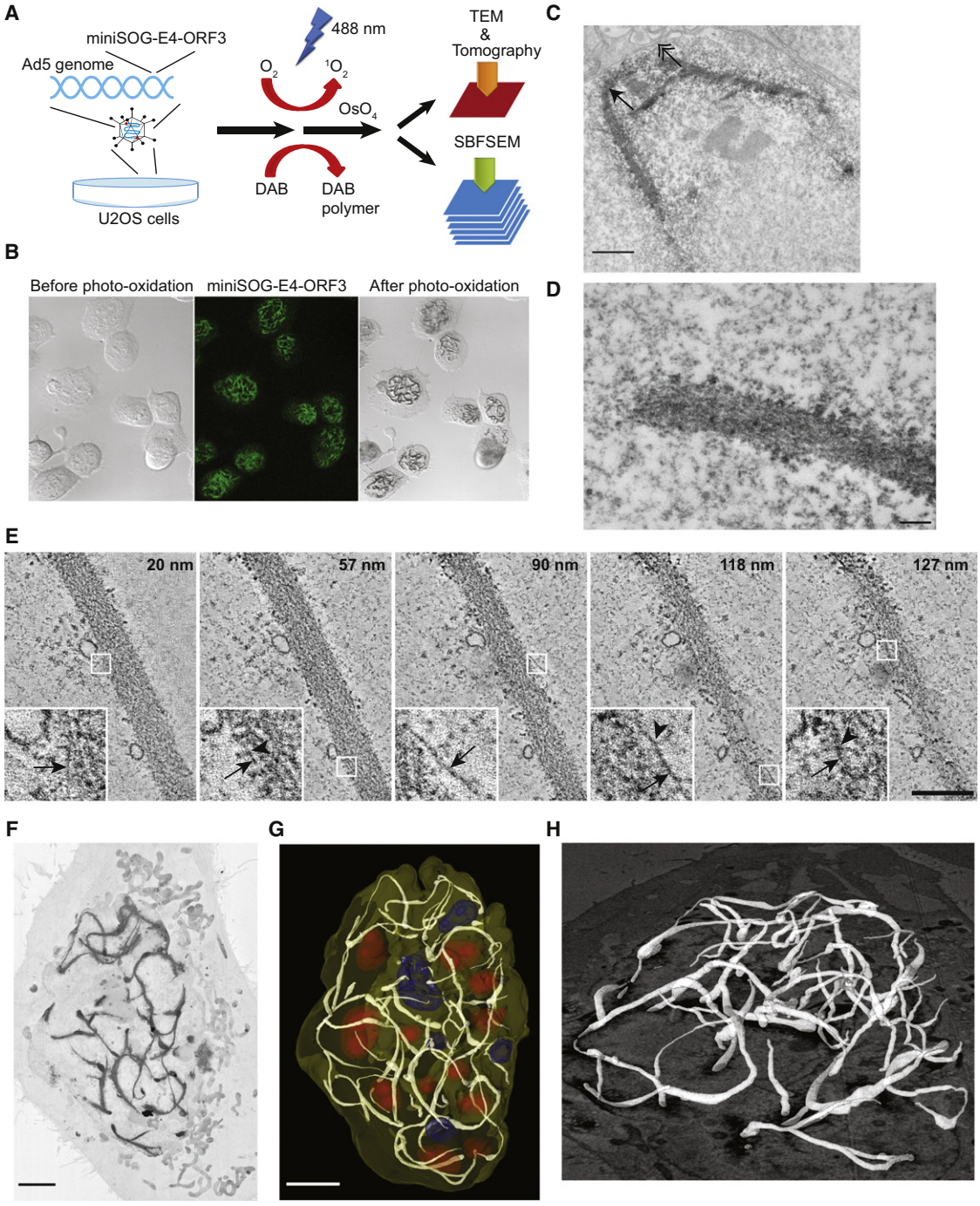

Figure 5. EM Ultrastructure of E4-ORF3 Polymer Assemblies and Nuclear Matrix

(A) U2OS cells were infected with Ad5 viruses that express miniSOG-E4-ORF3, photooxidized, and imaged by TEM, tomography, and SBFSEM.

(B) MiniSOG-E4-ORF3 prior to photooxidation (left: transmitted light; middle: fluorescence) and postphotooxidation (right: transmitted light).

(C and D) TEM images of E4-ORF3 assemblies (black arrow). Nuclear membrane (double arrow). Scale bars, 500 nm (C) and 100 nm (D).

(E) Individual cross sections (each 5 Å thick) of an E4-ORF3 tomogram volume (from top) with inset panel zooms. Arrows indicate linear assemblies; arrowheads indicate branched junctions. Scale bar, 200 nm.

(F) SBFSEM of E4-ORF3 in which 150 serial section images (each 60 nm thick) were reconstructed. Scale bar, 1 μm.

(G and H) Segmentation of SBFSEM data set. E4-ORF3 is in white, nucleoli in blue, viral replication domains are in red, and the nuclear membrane is in yellow. Scale bar, 5 μm.

See also Figure S4 and Movies S1, S2, S3, and S4.

E4-ORF3 polymer networks through the entire nuclear volume, we used serial block-face scanning electron microscopy (SBFSEM) (Denk and Horstmann, 2004). Images of 150 consecutive 60 nm sections were acquired from the bottom to the top of infected cells (Figures 5F–5H and S4B; Movies S2, S3, and S4). E4-ORF3 forms a network that circumnavigates the nucleoli and creates physical partitions around viral DNA replication domains (Figures 5G and S4C; Movie S4). The E4-ORF3 polymer networks have distinct topologies in individual cells (Movies S2 and S3), project in multiple dimensions, and have variable diameters, ranging from 60 to 710 nm in different places (Figure S4D). We conclude that E4-ORF3 assembles in multiple ways to form a disordered protein superstructure and 3D polymer network that physically partitions the nucleus.

E4-ORF3 Higher-Order Oligomerization Is Critical for Inactivating Disparate Tumor Suppressors and Facilitating Viral Replication

These data beg the question if E4-ORF3 assembly is required for its biological functions and interactions in viral replication. In adenovirus infection, E4-ORF3 and E1B-55K early viral oncoproteins have overlapping functions in inactivating p53 and MRN (Soria et al., 2010; Stracker et al., 2002). Therefore, to determine if E4-ORF3 higher-order assembly is necessary for p53 inactivation, we engineered adenoviruses that have an E1B-55K deletion and an N82A mutation in E4-ORF3. As expected, in ΔE1B-55K-infected primary cells, WT E4-ORF3 assembles a nuclear scaffold and prevents p53-activated transcription of *p21* and *MDM2* (Figures 6A and S5) (Soria et al., 2010). However, in ΔE1B-55K/E4-ORF3 N82A-infected cells, E4-ORF3 is unable to assemble a nuclear scaffold and inactivate p53 targets (Figures 6A and S5). Furthermore, E4-ORF3 N82A also fails to disrupt PML bodies (Figure 6B) or mislocalize NBS1 (a key component of the MRN complex) (Figure 6C). Consistent with this, ΔE1B-55K/E4-ORF3 N82A viruses are profoundly defective and do not form E2A viral DNA replication domains or express viral capsid proteins (Figures 6D and 6E). These data strongly suggest that the higher-order assembly of E4-ORF3 dimers is a unifying mechanism that is required for E4-ORF3's functions in inactivating disparate tumor suppressors and driving pathological viral replication.

E4-ORF3 Higher-Order Oligomerization Creates Avidity-Driven Interactions with PML and an Emergent MRN Binding Interface

We hypothesized that E4-ORF3 higher-order oligomerization is required for creating emergent binding sites and/or avidity-driven interactions with cellular partners (Figure 7A). The assembly of E4-ORF3 into a polymer would substantially reduce the "off-rate" of possible low-affinity interactions between individual E4-ORF3 dimer units and cellular partners by using multiple interaction points. Avidity-driven interactions require both partners to have multivalent binding sites (Mammen et al., 1998). Strikingly, PML is an oligomeric protein that forms nuclear "bodies" (Bernardi and Pandolfi, 2007), and the MRN complex assembles into foci at DNA breaks (D'Amours and Jackson, 2002).

We reasoned that if polymerization is critical for avidity-driven interactions, then E4-ORF3 N82A dimers that are engineered to assemble a higher-order superstructure through an independent oligomerization mechanism would bind and mislocalize PML and MRN (Figure 7B). Lamin A/C is a cellular protein that assembles 32-mer to form the nuclear lamina, an intermediate filament network (Herrmann et al., 2007). Therefore, to test our hypothesis, we created a protein fusion between Lamin A/C and E4-ORF3 N82A. Lamin A/C-E4-ORF3 N82A assembles into a nuclear superstructure that is distinct from Lamin A/C, WT E4-ORF3, and E4-ORF3 N82A (Figure 7C). Lamin A/C-E4-ORF3 N82A forms ring-like cylinders through the nucleus that disrupt and mislocalize PML. Thus, E4-ORF3 N82A mutants are perfectly capable of binding and mislocalizing PML when they are assembled into a higher-order oligomer by Lamin A/C fusions. We conclude that the higher-order assembly of E4-ORF3 creates avidity-driven interactions that capture and disrupt PML bodies.

In contrast to PML, Lamin A/C-E4-ORF3 N82A does not bind and mislocalize NBS1 (Figure 7D). This suggested that the higher-order assembly of E4-ORF3 dimers through C-terminal tail swapping is specifically required for interactions with MRN. Previously, I^{104} was implicated as a key residue that underlies the differential ability of Ad5 E4-ORF3 to bind and mislocalize MRN (Carson et al., 2009). In the E4-ORF3 N82* dimer structure, I^{104} is solvent exposed in a random coil region between the hinge residues and β4 in the C-terminal tail (Figure 7E). Thus, I^{104} is on the surface and available for binding in E4-ORF3 N82* dimers. However, this is not sufficient for MRN binding, even as part of a Lamin A/C-E4-ORF3 N82A avidity surface (Figure 7D).

Therefore, we hypothesized that I^{104} is part of an emergent MRN binding interface that is formed upon swapping of the C-terminal tails between E4-ORF3 dimer units (Figure 7E). To test this, we performed alanine-scanning mutagenesis of the residues in the random coil of the C-terminal tail (Figures 7E and S6A). V101A, H102A, I104A, and D105A mutations ablate E4-ORF3 interactions with NBS1 (Figures 7E and S6A). Furthermore, L103A prevents not only NBS1 binding but also E4-ORF3 assembly (Figures 7E and S6A). This suggests that L^{103} is important for secondary oligomeric interactions that favor and stabilize the "swapped" state. Finally, we show that the fusion of the C-terminal tail alone to Lamin A/C is not sufficient to mislocalize NBS1 to the nuclear lamina (Figure S6B). Together, these data suggest that C-terminal tail swaps create an emergent interface at residues V^{101}–D^{105} that is critical for MRN binding and E4-ORF3 assembly.

DISCUSSION

Adenovirus early protein interactions have led to the discovery of many of the critical cellular growth regulatory targets and mechanisms. However, the structural basis for their multiple functions and interactions has remained elusive due to the paucity of high-resolution structural information. Here, we determine the crystal structure of E4-ORF3 at 2.1 Å resolution. E4-ORF3 is not a structural homolog of any known cellular proteins that form polymers or that function in the p53, DNA damage, PML, or TRIM24 tumor suppressor pathways. However, E4-ORF3 shares a similar dimeric motif with HPV16 E2 DBD and EBNA1 DBD, which are from unrelated viruses. This raises the

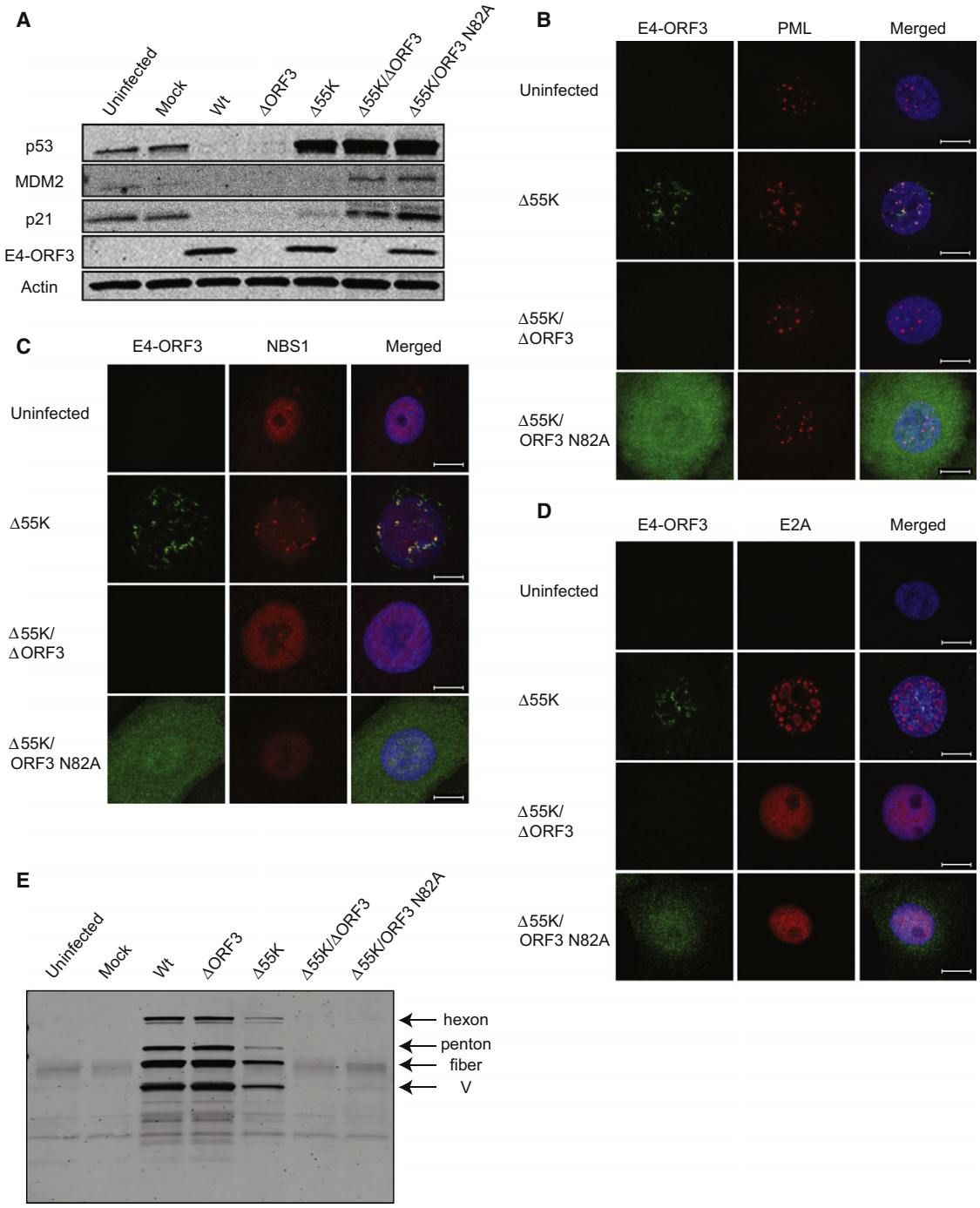

Figure 6. E4-ORF3 Higher-Order Oligomerization Is Critical for Inactivating Disparate Tumor Suppressors and Facilitating Viral Replication

(A) Primary SAECs were infected with either mock, Ad5 (WT), ΔE4-ORF3, ΔE1B-55K, ΔE1B-55K/ΔE4-ORF3 or ΔE1B-55K/E4-ORF3 N82A viruses. Protein lysates were harvested at 36 hpi, normalized, and immunoblotted for p53, MDM2, and p21. β-Actin is a loading control.

(B–D) Confocal images of infected SAECs immunostained for E4-ORF3 (green) and (B) PML (red), (C) NBS1 (red), (D) E2A viral replication domains (red). Scale bar, 10 μm.

(E) As per (A), except lysates were immunoblotted for Ad5 capsid proteins.

See also Figure S5.

intriguing possibility that these disparate viral proteins evolved from a common ancestor. Alternatively, they may have independently converged on the same structural solution because it represents an optimal combination in terms of minimizing protomer size and maximizing functional versatility.

To determine the structure and assembly mechanism of E4-ORF3, we exploited a dominant-negative oligomerization mutant (N82A). The crystal structure reveals the first-order subunit of E4-ORF3 polymer assemblies and dimerization interface. The N^{82} mutation is in the α3 helix, suggesting that it is at a critical oligomeric interface. However, mutagenesis studies did not reveal any additional residues in α3 that prevent E4-ORF3 assembly (Figures 3A and S3). We demonstrate that C-terminal tail deletions or L111K ablates the dominant-negative effects of N82A mutants and enables coassembly with WT E4-ORF3 (Figures 3D and 3E). Thus, N82A mutations do not directly prevent the assembly and stacking of WT E4-ORF3 when the β core is made available for intermolecular interactions.

Our data suggest that N^{82} mutations result in tertiary conformational changes that alter C-terminal tail interactions with the β core, thereby preventing β4 exchanges that drive higher-order assembly. This is consistent with our mutational analyses, which indicate that in contrast to the N82* crystal structure, in WT E4-ORF3 the β4 strand is extended and completes the dimer β barrel (Figures 3E, 3G, 4B, and 4C). It is not clear why N^{82} mutations would have such a drastic effect on C-terminal tail interactions with the β core. One possibility is that N^{82} mutations inhibit E4-ORF3 conformational heterogeneity thereby preventing intermolecular exchanges of the C-terminal tail. In such a model, N^{82} interactions could act as a molecular switch that modulates E4-ORF3 assembly. A precedent for this exists in other domain-swapped proteins, where conformational heterogeneity has been reported to facilitate exchanges, for example, the β4 strand of CKS1 (Seeliger et al., 2005). In future studies, a cocrystal structure of E4-ORF3 N82* with WT E4-ORF3 would help to clarify the molecular interactions of N^{82} in E4-ORF3 assembly.

Together, our studies suggest a model in which E4-ORF3 dimers coassemble through a combination of both reciprocal and nonreciprocal swapping of their C-terminal tails (Figure 4E). Reciprocal exchanges would result in more linear assemblies and nonreciprocal swapping in branched chains. Avidity interactions between oligomer chains would further drive assembly and result in variable arrangements and loose stacking requirements. This would rationalize the unusual ability of E4-ORF3 to assemble even when it is fused to miniSOG or GFP (Figures 1B and 5B), which is indicative of relaxed packing constraints.

The EM ultrastructure of E4-ORF3 polymer bundles is, for the most part, consistent with our model (Figures 4E and 5E; Movie S1). A tomogram reveals that E4-ORF3 assemblies are a disordered weave of individual oligomer threads that associate with one another in no fixed geometric arrangement. Although branching is observed, the oligomer threads exhibit a predominantly linear configuration. This suggests that reciprocal exchanges between E4-ORF3 dimer units are favored over nonreciprocal swaps. In other 3D domain-swapped proteins, reciprocal exchanges result in juxtaposed hinge residues that interact with one another to stabilize the "swapped" state (Liu et al., 2011). The random coil region adjacent to the hinge is a candidate for forming such a secondary oligomeric interface, as evidenced by the effects of L103A mutations in preventing E4-ORF3 assembly (Figure S6A). If a secondary L^{103} oligomeric interface is formed between residues in adjacent C-terminal tails, this would potentially favor reciprocal over nonreciprocal exchanges. Based on the crystal structure, L103A mutants would at least form dimers and be an interesting candidate for structural determination. No doubt, future studies will test these various models and the role of the random coil region and C-terminal tail in driving E4-ORF3 assembly and binding with cellular proteins.

The SBFSEM reconstructions show that E4-ORF3 forms a network of cables that physically separate viral replication domains from cellular nucleoli and chromatin (Figure 5G; Movie S4). E4-ORF3 specifically silences p53 target genes (Soria et al., 2010), but the E4-ORF3 nuclear network in each cell is distinct (Movies S2 and S3). One possible explanation is that E4-ORF3 assembly nucleates at specific points and then expands into the interchromatin space, which is more variable. Concentrating E4-ORF3 at specific loci would also create a crowded molecular environment that favors 3D domain swapping (Liu and Eisenberg, 2002). Thus, the sites of E4-ORF3 nucleation could unveil an underlying nuclear organization.

The E4-ORF3 nuclear polymer network is akin to a semisolid interaction matrix that would not be expected to exhibit traditional diffusion kinetics. The interactions of such a polyvalent matrix with its binding partners could exceed that of avidity and affinity-driven interactions. Such "matricity"-driven interactions have previously been described for clathrin, in which multiple weak binding sites form a dominant chelating surface upon polymerization (Schmid et al., 2006). E4-ORF3 assembly is required for its functions in inactivating p53, PML, MRN, and driving viral replication (Figure 6). We show that the assembly of E4-ORF3 creates avidity-driven interactions with PML and an MRN binding interface between residues V^{101} and D^{105} in the C-terminal tail (Figure 7). The emergent interactions of E4-ORF3 polymers explain a central paradox, namely why cellular binding partners do not prevent E4-ORF3 polymerization. The answer is that E4-ORF3 interactions require assembly. We conclude that E4-ORF3 binds to PML and MRN via two distinct molecular mechanisms, which are emergent functions of its higher-order oligomerization.

Our studies reveal an elegant structural solution whereby a small-ordered protein forms a dominant protein interaction matrix to capture and disrupt multiple large cellular protein complexes (Figure 7F). In general, multifunctional cellular protein hubs are large with multiple modular domains (Patil et al., 2010) and/or intrinsically disordered regions (Dunker et al., 2005) that enable them to bind many different partners simultaneously. The archetypal adenovirus oncoprotein, E1A, is mostly unstructured and uses intrinsically disordered short peptide motifs to bind multiple cellular partners (Ferreon et al., 2009; Pelka et al., 2008). E4-ORF3 flouts these conventions and instead uses a small domain to assemble a disordered protein superstructure that has multiple different binding sites. Thus, E4-ORF3 represents a new type of multifunctional hub and protein polymer that redefines the possibilities and potential for such structures.

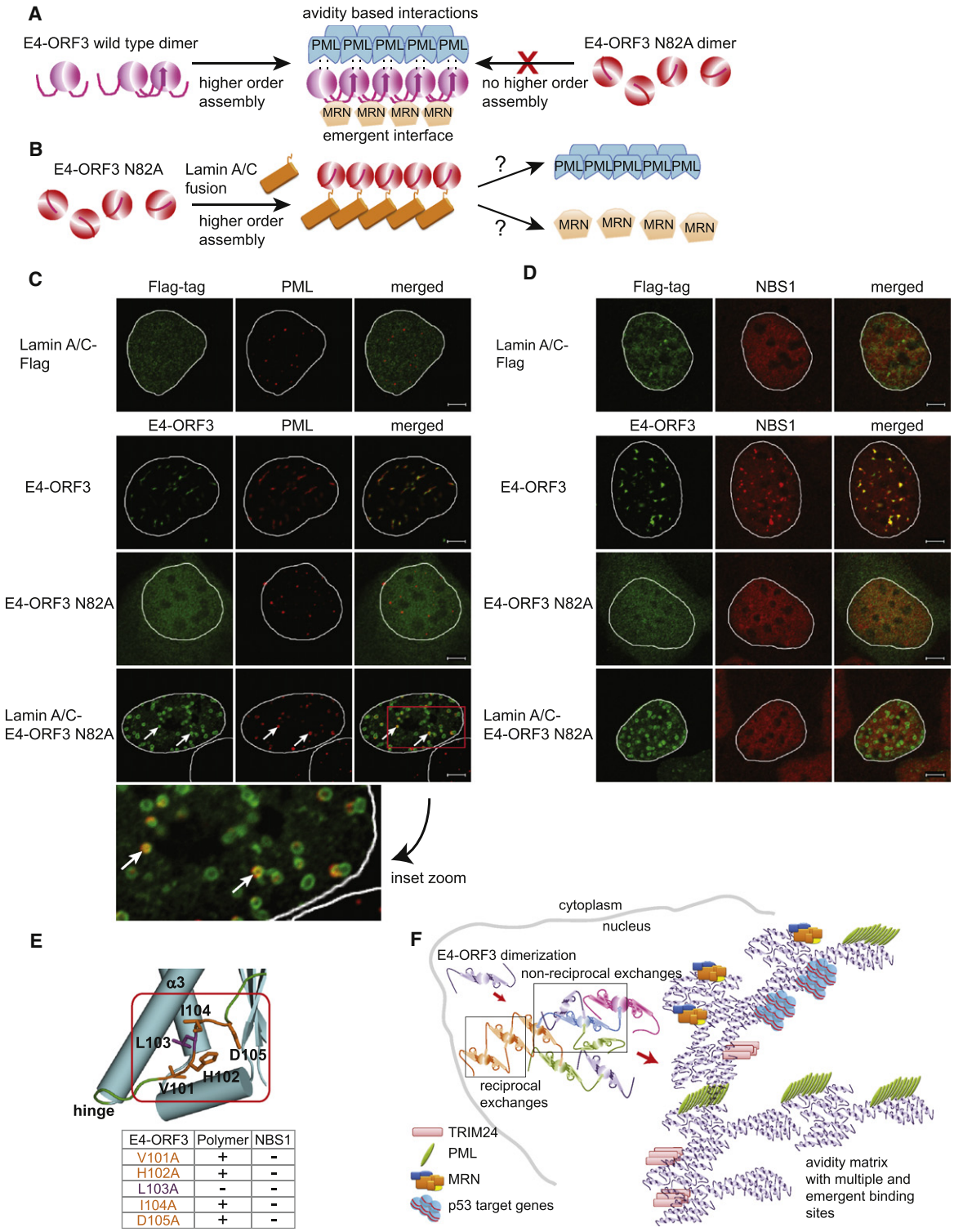

E4-ORF3	Polymer	NBS1
V101A	+	-
H102A	+	-
L103A	-	-
I104A	+	-
D105A	+	-

Figure 7. E4-ORF3 Assembly Creates Avidity-Driven Interactions with PML and an Emergent MRN Binding Site

(A) Models showing E4-ORF3 assembly is required to create emergent binding sites and/or avidity-based interactions with PML and MRN tumor suppressor complexes.

(B) To test this model, E4-ORF3 N82A was assembled by fusing it to an independent oligomeric protein, Lamin A/C (orange).

(C) U2OS cells transfected with either Lamin A/C-Flag, E4-ORF3, E4-ORF3 N82A or Lamin A/C-E4-ORF3 N82A fusions (green) and immunostained for PML (red) or (D) NBS1 (red). The nucleus is traced with a white line. Images are a single confocal slice. Scale bars, 5 μm.

Although E4-ORF3 is the first complete adenoviral early oncoprotein structure to be solved, we propose that viral early proteins in general may offset their limited surface areas by assembling different oligomeric complexes to usurp cellular protein interactions. The same principles revealed by E4-ORF3's structure-function are presaged by organic chemists' design of multivalent dendrimers to target cell surface ligands, where multiple weak contacts in a flexible scaffold are more efficient and selective than precise structures with stronger individual interactions (Martos et al., 2008). Finally, the structure of E4-ORF3 provides a rational basis for identifying new protein interaction surfaces that target critical tumor suppressors.

EXPERIMENTAL PROCEDURES

Cells, Plasmids, Transfections, and Viral Infections

Primary small airway epithelial cells (SAECs) were cultured and infected using established conditions (Soria et al., 2010). Protein lysates from infected cells were normalized and analyzed by western blotting. U2OS cells were transfected using Lipofectamine 2000 (Invitrogen). A 1:1 mix of WT and mutant E4-ORF3 plasmids was used. Refer to Extended Experimental Procedures for additional details.

Immunofluorescence

Cells were fixed in 4% paraformaldehyde and stained using established conditions (Soria et al., 2010). Images were acquired using a Zeiss LSM710 confocal microscope and Zeiss Elyra S.1 super-resolution-structured illumination microscope. Refer to Extended Experimental Procedures for additional details.

Expression of E4-ORF3 in *Nicotiana benthamiana*

mGFP5 and E4-ORF3-mGFP5 C-terminal fusion constructs were transformed into the *Agrobacterium* strain ASE and used for infiltration of *Nicotiana benthamiana* as previously described by Sparkes et al. (2006). Leaf plugs were harvested at 54 hr and stained with SCRI Renaissance 2200. Images were acquired using a 40× objective and are maximum projections of 22 optical slices.

Bacterial Protein Expression and Purification

E4-ORF3 constructs were expressed in the Rosetta *E. coli* strain (Novagen). 6×-his-tagged proteins were purified using QIAGEN Ni-NTA Superflow Sepharose and a Superdex 200 16/60 size exclusion column. Additional details can be found in Extended Experimental Procedures.

Crystallization

Seleno-methionine-labeled E4-ORF3 N82E/C71S/C86S was concentrated to 14.6 mg/ml and crystallized by hanging drop in 0.1 M HEPES (pH 7.0), 15% PEG 10,000, and 8% ethylene glycol with 1 μl protein solution and 1 μl precipitant solution. Crystals appear within 2 weeks. The crystals were flash frozen in the same buffer with 20% PEG 10,000.

Data Collection and Structure Refinement

Diffraction data were collected for a SeMet crystal at Stanford Synchrotron Radiation Lightsource beamline 9-2 to 2.06 Å. The crystal structure of E4-ORF3 was solved by single-wavelength anomalous dispersion using the selenium signal. Refinement of the structure was completed after multiple cycles, and noncrystallographic symmetry restraints were not applied. Data processing and refinement statistics are listed in Table S1. Final R and R_{free} values are 0.212 and 0.256, respectively. All figures were prepared with PyMOL (Delano, 2002). Additional details are in Extended Experimental Procedures.

Dali and PDBeFOLD Homology Search

The structural coordinates of E4-ORF3 N82* were used to search the Dali (http://ekhidna.biocenter.helsinki.fi/dali_server/) and PDBeFOLD servers (http://www.ebi.ac.uk/msd-srv/ssm). For PDBeFOLD, shared secondary structural element between query and target proteins was set at 60%.

Correlated Light and EM

Cells were grown and infected on MatTek dishes and fixed with 2% glutaraldehyde. Regions of interest were selected using a Leica SPE-II microscope, photo-oxidized, and stained as described previously (Shu et al., 2011). Ultrathin sections were cut and electron micrographs recorded using a 1200 TEM (JEOL). For SBFSEM, a 3View system (Gatan) mounted in a Quanta FEG variable pressure scanning electron microscope (FEI) with an oscillating diamond knife was used to image blocks at 60 nm increments. Segmentation was performed using IMOD (Kremer et al., 1996). Refer to Extended Experimental Procedures for additional details.

Electron Tomography

Sections were cut at 250 nm thickness and mounted on 75 mesh copper grids. Images were recorded at 40,000× magnification and angular increments of 2° from −60° to +60° using a JEOL 4000EX intermediate voltage electron microscope operated at 400kV. Images were aligned and reconstructed using IMOD, TxBR, and Amira. The reconstructed tomogram comprises 500 computational slices (each 0.5 nm). Refer to Extended Experimental Procedures for additional details.

ACCESSION NUMBERS

The Protein Data Bank accession number for the E4-ORF3 atomic coordinates and structure factors reported in this paper is 4DJB.

SUPPLEMENTAL INFORMATION

Supplemental Information includes Extended Experimental Procedures, six figures, one table, and four movies and can be found with this article online at http://dx.doi.org/10.1016/j.cell.2012.08.035.

ACKNOWLEDGMENTS

We thank F. McCormick, T. Hunter, J. Chory, V. Lundblad, J. Young, I. Verma, and members of the C.C.O. laboratory for all of their support, insights, and helpful comments. We thank S. Phan and M. Terada for help with EM tomography. This work was supported by the following NIH grants awarded to the Salk Institute: CA137094 to C.C.O., a T32 fellowship (CA009370) to H.D.O., P30CA014195 provides support for the Salk Cancer Center, P30NS057096 supports in part the Salk X-ray equipment. The National Center for Microscopy contributions were supported by NIH awards 5P41RR004050 and P41GM103412-24 to M.H.E. The MiniSOG probe development was supported under RO1GM086197 (to R.Y.T. and M.H.E.). C.C.O. is also supported by the William Scandling Developmental Chair and young investigator awards from the American Cancer Society, the Sontag Foundation, the Arnold and Mabel Beckman Foundation, and the Anna Fuller Fund.

Received: December 22, 2011
Revised: May 10, 2012
Accepted: August 16, 2012
Published: October 11, 2012

(E) The top panel shows residues V^{101}–D^{105} in the C-terminal tail of the E4-ORF3 N82* dimer structure. The bottom panel is a summary of mutational analysis, which indicates that they form an emergent MRN binding site and secondary oligomeric interface upon WT E4-ORF3 assembly.
(F) E4-ORF3 forms dimers that further assemble in many different configurations to form a multivalent matrix that captures PML, TRIM24, and MRN tumor suppressor complexes and silences p53 target promoters in cellular chromatin.
See also Figure S6.

REFERENCES

Aebi, U., Millonig, R., Salvo, H., and Engel, A. (1986). The three-dimensional structure of the actin filament revisited. Ann. N Y Acad. Sci. *483*, 100–119.

Bennett, M.J., Sawaya, M.R., and Eisenberg, D. (2006). Deposition diseases and 3D domain swapping. Structure *14*, 811–824.

Berk, A.J. (2007). Adenoviridae: the viruses and their replication. In Fields Virology, D.M. Knipe and P.M. Howley, eds. (Philadelphia: Lippincott Williams & Wilkins and Wolters Kluwer), pp. 2355–2394.

Bernardi, R., and Pandolfi, P.P. (2007). Structure, dynamics and functions of promyelocytic leukaemia nuclear bodies. Nat. Rev. Mol. Cell Biol. *8*, 1006–1016.

Bochkarev, A., Barwell, J.A., Pfuetzner, R.A., Furey, W., Jr., Edwards, A.M., and Frappier, L. (1995). Crystal structure of the DNA-binding domain of the Epstein-Barr virus origin-binding protein EBNA 1. Cell *83*, 39–46.

Brendel, V., and Karlin, S. (1989). Association of charge clusters with functional domains of cellular transcription factors. Proc. Natl. Acad. Sci. USA *86*, 5698–5702.

Carson, C.T., Orazio, N.I., Lee, D.V., Suh, J., Bekker-Jensen, S., Araujo, F.D., Lakdawala, S.S., Lilley, C.E., Bartek, J., Lukas, J., and Weitzman, M.D. (2009). Mislocalization of the MRN complex prevents ATR signaling during adenovirus infection. EMBO J. *28*, 652–662.

Carvalho, T., Seeler, J.S., Ohman, K., Jordan, P., Pettersson, U., Akusjärvi, G., Carmo-Fonseca, M., and Dejean, A. (1995). Targeting of adenovirus E1A and E4-ORF3 proteins to nuclear matrix-associated PML bodies. J. Cell Biol. *131*, 45–56.

Chhabra, E.S., and Higgs, H.N. (2007). The many faces of actin: matching assembly factors with cellular structures. Nat. Cell Biol. *9*, 1110–1121.

D'Amours, D., and Jackson, S.P. (2002). The Mre11 complex: at the crossroads of dna repair and checkpoint signalling. Nat. Rev. Mol. Cell Biol. *3*, 317–327.

Delano, W.L. (2002). The PyMOL Molecular Graphics System (San Carlos, CA: DeLano Scientific).

Denk, W., and Horstmann, H. (2004). Serial block-face scanning electron microscopy to reconstruct three-dimensional tissue nanostructure. PLoS Biol. *2*, e329.

Doucas, V., Ishov, A.M., Romo, A., Juguilon, H., Weitzman, M.D., Evans, R.M., and Maul, G.G. (1996). Adenovirus replication is coupled with the dynamic properties of the PML nuclear structure. Genes Dev. *10*, 196–207.

Dunker, A.K., Cortese, M.S., Romero, P., Iakoucheva, L.M., and Uversky, V.N. (2005). Flexible nets. The roles of intrinsic disorder in protein interaction networks. FEBS J. *272*, 5129–5148.

Evans, J.D., and Hearing, P. (2003). Distinct roles of the Adenovirus E4 ORF3 protein in viral DNA replication and inhibition of genome concatenation. J. Virol. *77*, 5295–5304.

Ferreon, J.C., Martinez-Yamout, M.A., Dyson, H.J., and Wright, P.E. (2009). Structural basis for subversion of cellular control mechanisms by the adenoviral E1A oncoprotein. Proc. Natl. Acad. Sci. USA *106*, 13260–13265.

Giri, I., and Yaniv, M. (1988). Structural and mutational analysis of E2 transactivating proteins of papillomaviruses reveals three distinct functional domains. EMBO J. *7*, 2823–2829.

Gustafsson, M.G. (2000). Surpassing the lateral resolution limit by a factor of two using structured illumination microscopy. J. Microsc. *198*, 82–87.

Haynes, C., Oldfield, C.J., Ji, F., Klitgord, N., Cusick, M.E., Radivojac, P., Uversky, V.N., Vidal, M., and Iakoucheva, L.M. (2006). Intrinsic disorder is a common feature of hub proteins from four eukaryotic interactomes. PLoS Comput. Biol. *2*, e100.

Hegde, R.S., and Androphy, E.J. (1998). Crystal structure of the E2 DNA-binding domain from human papillomavirus type 16: implications for its DNA binding-site selection mechanism. J. Mol. Biol. *284*, 1479–1489.

Herrmann, H., Bär, H., Kreplak, L., Strelkov, S.V., and Aebi, U. (2007). Intermediate filaments: from cell architecture to nanomechanics. Nat. Rev. Mol. Cell Biol. *8*, 562–573.

Holm, L., and Rosenström, P. (2010). Dali server: conservation mapping in 3D. Nucleic Acids Res. *38*(*Web Server issue*), W545–W549.

Hoppe, A., Beech, S.J., Dimmock, J., and Leppard, K.N. (2006). Interaction of the adenovirus type 5 E4 Orf3 protein with promyelocytic leukemia protein isoform II is required for ND10 disruption. J. Virol. *80*, 3042–3049.

Howard, J., and Hyman, A.A. (2003). Dynamics and mechanics of the microtubule plus end. Nature *422*, 753–758.

Khetchoumian, K., Teletin, M., Tisserand, J., Mark, M., Herquel, B., Ignat, M., Zucman-Rossi, J., Cammas, F., Lerouge, T., Thibault, C., et al. (2007). Loss of Trim24 (Tif1alpha) gene function confers oncogenic activity to retinoic acid receptor alpha. Nat. Genet. *39*, 1500–1506.

Kim, S.S., Tam, J.K., Wang, A.F., and Hegde, R.S. (2000). The structural basis of DNA target discrimination by papillomavirus E2 proteins. J. Biol. Chem. *275*, 31245–31254.

Kremer, J.R., Mastronarde, D.N., and McIntosh, J.R. (1996). Computer visualization of three-dimensional image data using IMOD. J. Struct. Biol. *116*, 71–76.

Krissinel, E., and Henrick, K. (2004). Secondary-structure matching (SSM), a new tool for fast protein structure alignment in three dimensions. Acta Crystallogr. D Biol. Crystallogr. *60*, 2256–2268.

Liu, C., Sawaya, M.R., and Eisenberg, D. (2011). β_2-microglobulin forms three-dimensional domain-swapped amyloid fibrils with disulfide linkages. Nat. Struct. Mol. Biol. *18*, 49–55.

Liu, Y., and Eisenberg, D. (2002). 3D domain swapping: as domains continue to swap. Protein Sci. *11*, 1285–1299.

Mammen, M., Choi, S.-K., and Whitesides, G.M. (1998). Polyvalent interactions in biological systems: implications for design and use of multivalent ligands and inhibitors. Angew. Chem. Int. Ed. Engl. *37*, 2754–2794.

Martos, V., Castreño, P., Valero, J., and de Mendoza, J. (2008). Binding to protein surfaces by supramolecular multivalent scaffolds. Curr. Opin. Chem. Biol. *12*, 698–706.

Morgan, C., Godman, G.C., Breitenfeld, P.M., and Rose, H.M. (1960). A correlative study by electron and light microscopy of the development of type 5 adenovirus. I. Electron microscopy. J. Exp. Med. *112*, 373–382.

Nordqvist, K., Ohman, K., and Akusjärvi, G. (1994). Human adenovirus encodes two proteins which have opposite effects on accumulation of alternatively spliced mRNAs. Mol. Cell. Biol. *14*, 437–445.

O'Shea, C.C. (2005). Viruses—seeking and destroying the tumor program. Oncogene *24*, 7640–7655.

Ou, H.D., May, A.P., and O'Shea, C.C. (2011). The critical protein interactions and structures that elicit growth deregulation in cancer and viral replication. Wiley Interdiscip. Rev. Syst. Biol. Med. *3*, 48–73.

Patil, A., Kinoshita, K., and Nakamura, H. (2010). Domain distribution and intrinsic disorder in hubs in the human protein-protein interaction network. Protein Sci. *19*, 1461–1468.

Pelka, P., Ablack, J.N., Fonseca, G.J., Yousef, A.F., and Mymryk, J.S. (2008). Intrinsic structural disorder in adenovirus E1A: a viral molecular hub linking multiple diverse processes. J. Virol. *82*, 7252–7263.

Ponstingl, H., Henrick, K., and Thornton, J.M. (2000). Discriminating between homodimeric and monomeric proteins in the crystalline state. Proteins *41*, 47–57.

Puvion-Dutilleul, F., Chelbi-Alix, M.K., Koken, M., Quignon, F., Puvion, E., and de Thé, H. (1995). Adenovirus infection induces rearrangements in the intranuclear distribution of the nuclear body-associated PML protein. Exp. Cell Res. *218*, 9–16.

Ronning, D.R., Guynet, C., Ton-Hoang, B., Perez, Z.N., Ghirlando, R., Chandler, M., and Dyda, F. (2005). Active site sharing and subterminal hairpin recognition in a new class of DNA transposases. Mol. Cell *20*, 143–154.

Schmid, E.M., Ford, M.G., Burtey, A., Praefcke, G.J., Peak-Chew, S.Y., Mills, I.G., Benmerah, A., and McMahon, H.T. (2006). Role of the AP2 beta-appendage hub in recruiting partners for clathrin-coated vesicle assembly. PLoS Biol. *4*, e262.

Scott, J.D., and Pawson, T. (2009). Cell signaling in space and time: where proteins come together and when they're apart. Science *326*, 1220–1224.

Seeliger, M.A., Spichty, M., Kelly, S.E., Bycroft, M., Freund, S.M., Karplus, M., and Itzhaki, L.S. (2005). Role of conformational heterogeneity in domain swapping and adapter function of the Cks proteins. J. Biol. Chem. *280*, 30448–30459.

Shu, X., Lev-Ram, V., Deerinck, T.J., Qi, Y., Ramko, E.B., Davidson, M.W., Jin, Y., Ellisman, M.H., and Tsien, R.Y. (2011). A genetically encoded tag for correlated light and electron microscopy of intact cells, tissues, and organisms. PLoS Biol. *9*, e1001041.

Sipe, J.D., and Cohen, A.S. (2000). Review: history of the amyloid fibril. J. Struct. Biol. *130*, 88–98.

Soria, C., Estermann, F.E., Espantman, K.C., and O'Shea, C.C. (2010). Heterochromatin silencing of p53 target genes by a small viral protein. Nature *466*, 1076–1081.

Sparkes, I.A., Runions, J., Kearns, A., and Hawes, C. (2006). Rapid, transient expression of fluorescent fusion proteins in tobacco plants and generation of stably transformed plants. Nat. Protoc. *1*, 2019–2025.

Stracker, T.H., Carson, C.T., and Weitzman, M.D. (2002). Adenovirus oncoproteins inactivate the Mre11-Rad50-NBS1 DNA repair complex. Nature *418*, 348–352.

Stracker, T.H., Lee, D.V., Carson, C.T., Araujo, F.D., Ornelles, D.A., and Weitzman, M.D. (2005). Serotype-specific reorganization of the Mre11 complex by adenoviral E4orf3 proteins. J. Virol. *79*, 6664–6673.

Ullman, A.J., Reich, N.C., and Hearing, P. (2007). Adenovirus E4 ORF3 protein inhibits the interferon-mediated antiviral response. J. Virol. *81*, 4744–4752.

Vidal, M., Cusick, M.E., and Barabási, A.L. (2011). Interactome networks and human disease. Cell *144*, 986–998.

Weitzman, M.D., and Ornelles, D.A. (2005). Inactivating intracellular antiviral responses during adenovirus infection. Oncogene *24*, 7686–7696.

Wells, J.A., and McClendon, C.L. (2007). Reaching for high-hanging fruit in drug discovery at protein-protein interfaces. Nature *450*, 1001–1009.

Yondola, M.A., and Hearing, P. (2007). The adenovirus E4 ORF3 protein binds and reorganizes the TRIM family member transcriptional intermediary factor 1 alpha. J. Virol. *81*, 4264–4271.